Nonheme Iron Hot Paper

How to cite: *Angew. Chem. Int. Ed.* **2021**, *60*, 26281 – 26286
International Edition: doi.org/10.1002/anie.202112683
German Edition: doi.org/10.1002/ange.202112683

Rapid Iron(III)–Fluoride-Mediated Hydrogen Atom Transfer

*Chakadola Panda, Lorna M. Doyle, Robert Gericke, and Aidan R. McDonald**

Abstract: *We anticipate high-valent metal–fluoride species will be highly effective hydrogen atom transfer (HAT) oxidants because of the magnitude of the H–F bond (in the product) that drives HAT oxidation. We prepared a dimeric $Fe^{III}(F)$–F–$Fe^{III}(F)$ complex (**1**) by reacting $[Fe^{II}(NCCH_3)_2(TPA)](ClO_4)_2$ (TPA = tris(2-pyridylmethyl)amine) with difluoro(phenyl)-λ^3-iodane (difluoroiodobenzene). **1** was a sluggish oxidant, however, it was readily activated by reaction with Lewis or Brønsted acids to yield a monomeric $[Fe^{III}(TPA)(F)(X)]^+$ complex (**2**) where X = F/OTf. **1** and **2** were characterized using NMR, EPR, UV/Vis, and FT-IR spectroscopies and mass spectrometry. **2** was a remarkably reactive Fe^{III} reagent for oxidative C–H activation, demonstrating reaction rates for hydrocarbon HAT comparable to the most reactive Fe^{III} and Fe^{IV} oxidants.*

Introduction

The functionalization of alkanes via C–H bond activation is critically important from industrial and environmental perspectives.[1] Owing to their relatively strong C(sp^3)–H bonds, practical large-scale synthetic applications of oxidative C–H activation have been hindered.[2] Nature has evolved to perform such transformations by employing iron enzymes under ambient conditions. High-valent iron–hydroxide (Fe–OH) or iron–oxo (Fe=O) oxidants drive such reactions both in enzymes and their synthetic models.[3] These oxidants perform a rate-limiting hydrogen atom transfer (HAT, a form of concerted proton-coupled electron transfer, PCET) oxidation of substrate C–H bonds. The driving force for this reaction is the strength of the O–H bond in the reduced product, an Fe–OH_2 or Fe–OH species, respectively. To date, the synthetic Fe–OH_2 or Fe–OH that have been characterized display O–H bond dissociation energy (BDE_{O-H}) values ≤ 90 kcal mol^{-1} meaning current oxidants generally don't activate strong C–H bonds *or* react at less than optimal rates.[4] Our goal is to design oxidants that will have the highest possible driving force for C–H activation.

To this end we are exploring high-valent metal–halides for HAT oxidation of hydrocarbons.[5] We postulate that the products of HAT by these oxidants are the one-electron reduced metal and the corresponding hydrohalic acid (H–X). The magnitude of H–X bond dissociation energy (BDE_{X-H}) would thus provide the driving force for C–H activation. The BDE_{X-H} values for H–F/Cl are considerably higher than those measured for Fe–OH_x species so far ($BDE_{H-F} = 135$ kcal mol^{-1}; $BDE_{H-Cl} = 103$ kcal mol^{-1}).[6] This discussion omits the role of the Fe–O/X bond in the oxidant, which will also affect the thermodynamic driving force for C–H activation. In the current manuscript we focus on the role of the magnitude of BDE_{H-X} in the product. Metal–fluoride oxidants thus appear to be ideal candidates to activate strong C–H bonds at high rates. Indeed, we found that substituting F for Cl in Ni^{III}–X increased the rate of reaction by three orders of magnitude.[5b] Doyle and co-workers demonstrated Ni–Cl complexes were effective HAT oxidants under irradiation,[7] while Nocera and co-workers demonstrated Fe^{III}–Cl species yielded a chlorine radical (Cl·) that acted as an HAT oxidant.[8] High-valent metal–halides are thus effective oxidants that could activate the strongest of C–H bonds under the right conditions.

An abundance of synthetic Fe^{IV}=O oxidants has now been accumulated,[3a,c,d,9] providing insight into their physical and reactivity properties.[1b,2,3c,9a,10] Fe^{III} oxidants that perform oxidative activation of C–H bonds are rare,[11] with most studies limited to synthesis and electronic structure determination.[12] Several complexes of the formula $[Fe^{III}(OR)(L)]$ (L = ligand and R = H/alkyl) have been targeted as models of lipoxygenase but were shown to be sluggish HAT oxidants.[13] A recent Fe^{III}=O identified in the gas phase was incapable of activating C–H bonds.[14] Very few Fe^{III} oxidants can match Fe^{IV}=O species in terms of the rates of C–H activation and the strength of the C–H bond that they can activate. Herein, we present an Fe^{III}–F complex that reacts at rates comparable to Fe^{IV}=O oxidants and outperforms the majority of Fe^{III} oxidants reported to date.

Results and Discussion

μ-Fluorido-diiron(III) complex **1** was synthesized by treating $[Fe^{II}(NCCH_3)_2(TPA)](ClO_4)_2$ (TPA = tris(2-pyridylmethyl)amine) with two molar equivalents of difluoro(phenyl)-λ^3-iodane (difluoroiodobenzene) at room temperature in CH_3CN (Scheme 1). Pale yellow crystals were

[*] Dr. C. Panda, L. M. Doyle, Dr. R. Gericke, Dr. A. R. McDonald
School of Chemistry, Trinity College Dublin
The University of Dublin
College Green, Dublin 2 (Ireland)
E-mail: aidan.mcdonald@tcd.ie
Dr. R. Gericke
Current address: Helmholtz-Zentrum Dresden-Rossendorf e. V.
Institute of Resource Ecology
Bautzner Landstrasse 400, 01328 Dresden (Germany)
Supporting information and the ORCID identification number(s) for the author(s) of this article can be found under: https://doi.org/10.1002/anie.202112683.

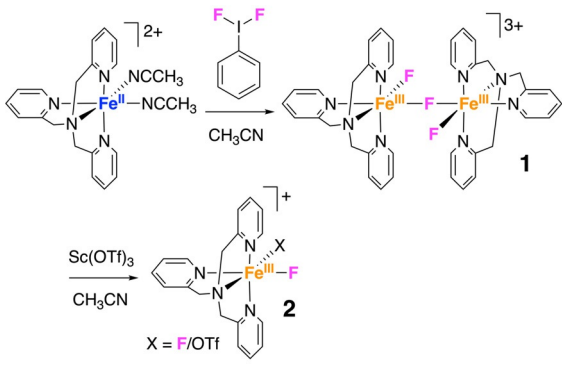

Scheme 1. Synthesis of compounds **1** and **2**, anions omitted for clarity.

isolated by diffusing diethyl ether (Et_2O) into the reaction mixture giving **1** in 45% yield. **1** crystallized in the triclinic crystal system as a tricationic species with three ClO_4^- counter anions (Figure 1).[15] The μ-F-atom serves as the center of inversion and the Fe1-F2-Fe1* angle was 180°. The μ-F–Fe bonds (Fe1–F2 = 1.957(1) Å) were slightly longer than the terminal Fe–F bonds (Fe1–F1; 1.826(2) Å). This is consistent with previous observations distinguishing terminal- (1.834(2) Å[16]) and μ-F (1.944(3) Å) atoms.[17]

The ^{1}H NMR of **1** displayed seven paramagnetically shifted signals (Figure S3). Eleven resonances would be expected based on the crystallographically determined structure, however, given the paramagnetic ion effect, it is expected that some resonances are overlapping/not identifiable. Similar ^{1}H NMR spectra have been obtained for a structurally analogous Fe^{III}(OH)–O–Fe^{III}(OH) complex supported by the same ligand.[18] An Evan's method magnetic moment measurement of 5.2 Bohr magnetons was obtained for **1** indicating the presence of four unpaired electrons in the ground state. The ^{19}F NMR spectrum of **1** showed a broad single signal at $\delta = -179$ ppm (Figure S4). The X-ray structure of **1** indicated two distinct F-atom environments, one would thus expect two resonances in the ^{19}F NMR, although the paramagnetic ion may cause these signals to coalesce or not be visible at all. NMR spectroscopy confirms that **1** is pure in solution and indicates that the Fe–F interaction remains intact.

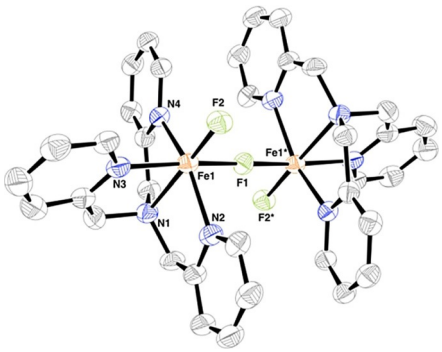

Figure 1. ORTEP of the tricationic species **1**.[15] ClO_4^- anions and H atoms have been omitted for clarity. Ellipsoids are drawn at 50% probability level.

The perpendicular mode X-band EPR spectrum of **1** displayed no signal, suggesting a diamagnetic species where both the Fe^{III} are antiferromagnetically coupled to each other (Figure S5). Therefore, we concluded that **1** remained as a dimer in solution. ESI-MS demonstrated two fragments at $m/z = 182.54$ and 384.08, which can be assigned to the dication $[Fe^{III}(F)(TPA)]^{2+}$ and monocation $[Fe^{III}(F)_2(TPA)]^+$, respectively (Figures S6–S8). We postulate that **1** was not stable under the ESI-MS instrumental conditions and underwent fragmentation into the mononuclear species. Similar ESI-MS-induced fragmentation of μ-oxo-diiron(IV) was previously reported.[19] The Fourier-transform infra-red (FT-IR) spectrum of **1** showed multiple signals including $\tilde{\nu} = 655$, 410 cm^{-1} that could be assigned to the bridging and terminal ν_{Fe-F} stretches (Figure S9). Terminal ν_{Fe-F} have been reported from $\tilde{\nu} = 400$–500 cm^{-1}, while asymmetric $\nu_{Fe-F-Fe}$ are proposed to fall in the higher energy region $\tilde{\nu} = 650$ cm^{-1}.[17b,20] We assign the peak at $\tilde{\nu} = 655$ cm^{-1} to the asymmetric $\nu_{Fe-F-Fe}$ stretch and the peak at $\tilde{\nu} = 410$ cm^{-1} to the terminal ν_{Fe-F} based on the above literature precedent and further experimentation below.

Previous work on $Fe^{II/III}$–F complexes has been limited to their electronic, structural, or magnetic properties.[17c,21] To the best of our knowledge, no such compounds have been explored for oxidation reactivity. We explored the reactivity of **1** as an oxidant towards C(sp^3)–H bond activation. The reaction between **1** and 1,4-cyclohexadiene (CHD, 10 equiv., 25 °C, Figure S10) was followed by electronic absorption spectroscopy using the shoulder at $\lambda = 310$ nm (Figure S2). This feature decreased slightly with a concomitant increase at $\lambda = 400$ nm (formation of Fe^{II} precursor; Figure S11), indicating a reaction may have occurred. The product of this reaction was benzene, obtained in 6% yield with respect to [**1**] according to ^{1}H NMR (Figure S12). The observation of benzene indicated **1** was a capable PCET oxidant. The very slow rate of oxidation, incomplete reaction, and the low yields of product led us to explore methods to activate this promising oxidant further.

We postulated that the addition of $Sc^{III}(OTf)_3$ (OTf = trifluoromethanesulfonate, triflate) might activate **1** to be a more effective PCET oxidant. It has been shown that the use of a Lewis acid can promote PCET reactivity.[22] Furthermore, the Lewis acid cleavage of a bis-μ-O-$Mn^{III}Mn^{IV}$ complex to form a mononuclear Mn^{IV}=O resulted in fast epoxidation of olefins.[23] Addition of $Sc^{III}(OTf)_3$ (2 equiv.) to a solution of **1** (0.1 mM, CH_3CN, 0 °C) generated a new species (**2**) with a band at $\lambda = 375$ nm (Scheme 1 and Figure 2). A titration of $Sc^{III}(OTf)_3$ with **1** suggested that two equivalents were necessary to obtain **2** in maximum yield. This equates to an Fe:Sc ratio of 1:1 in **2**, indicating that $Sc^{III}(OTf)_3$ may have broken the dimer to yield a monomer. **2** was stable at 0 °C (Figure S13), however, attempts to isolate single crystals of **2** for X-ray diffraction measurements were unsuccessful.

Brønsted acids are also known to activate M=O oxidants in an analogous fashion to Lewis acids.[22k] We reacted **1** (0.1 mM, CH_3CN, 0 °C; Figure S14) with a strong Brønsted acid, $HClO_4$ (2 equiv.), and observed very similar UV/Vis spectral changes as observed when Sc^{III} was added (i.e. the formation of **2**) but in lower yield. Additionally, **2** generated

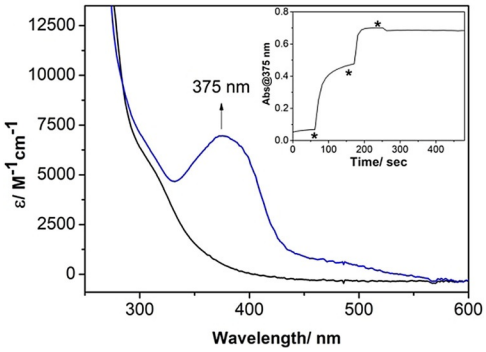

Figure 2. UV/Vis spectra for the addition of $Sc^{III}(OTf)_3$ to a solution of **1** (black trace, 0.1 mM, CH_3CN, 0 °C) to yield **2** (blue trace). Inset: Time trace of absorbance change at $\lambda = 375$ nm during the sequential titration of $Sc^{III}(OTf)_3$ (1 equiv. per titer). * = the point when each titer of $Sc^{III}(OTf)_3$ was added.

from $HClO_4$ decayed relatively rapidly with respect to **2** generated from Sc^{III} (Figure S14). We conclude that both Lewis acids and Brønsted acids cause the break-up of dimeric **1** to yield a monomeric species **2**. Lewis acids can react with adventitious water present in a reaction media thereby releasing strong Brønsted acids (HOTf for $Sc^{III}(OTf)_3$) which may be responsible for the formation of **2**.[27] Hence, we performed the reaction of **1** with $Sc^{III}(OTf)_3$ in the presence of 2% v/v water. Firstly, **1** did not react with water (a weak Brønsted acid). Secondly, we did not observe the formation of **2** (Figure S15), and therefore, we rule out the involvement of any adventitious water in the reaction media.

The X-band EPR spectrum of **2** exhibited a rhombic signal with $g = 2.70$, 2.40, and 1.53 (Figure 3). The average g-value $g_{av} = 2.21$ is indicative of a metal-based radical and such g-values have previously been ascribed to mononuclear $S = {}^1/_2$ Fe^{III} species.[24] For example, several heme and non-heme ligand supported $S = {}^1/_2$ Fe^{III} compounds with similar g-values to that of **2** have also been reported (Table S1).[25] Spin quantification was performed using 2,2,6,6-tetramethyl-1-piperidinyloxyl (TEMPO) as a reference (see Supporting Information for details), showing the yield of **2** was close to quantitative (75% ±10% with respect to [**1**]). EPR thus indicated the conversion of **1** to **2** represented the formation of a mononuclear $S = {}^1/_2$ Fe^{III} species in high yields.

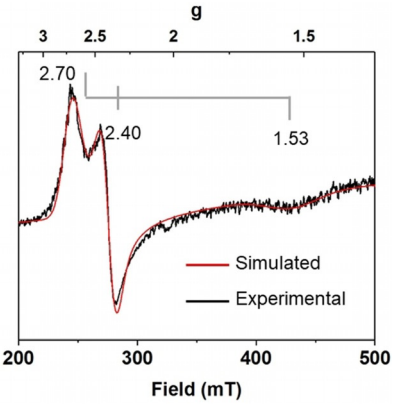

Figure 3. X-band EPR spectrum of **2** (black trace) obtained from the reaction of **1** (20 mM) and $Sc^{III}(OTf)_3$ in CH_3CN. Measured at 77 K, 9.2 GHz microwave frequency, 1.99 mW microwave power, and 0.3 mT modulation amplitude. Simulated spectrum for **2** (red trace; $g_x = 2.70$, $g_y = 2.40$, $g_z = 1.53$).

^{1}H NMR analysis of **2** displayed eight paramagnetically shifted signals (Figure S16). For a mononuclear [Fe(TPA)] complex, eleven resonances would again be expected. In comparison with **1**, the resonances for **2** were shifted to higher field, while they are also remarkably similar to other mononuclear $S = {}^1/_2$ Fe^{III} complexes supported by polypyridine ligands.[26] The spectrum was consistent with **2** being a pure mononuclear Fe^{III} complex supported by TPA and did not contain a mixture of paramagnetic species. ^{19}F NMR analysis showed only one signal at $\delta = -79$ ppm which can be assigned to the OTf counterion (derived from $Sc^{III}(OTf)_3$, Figure S17) and no signals that could be associated with the Fe^{III}–F moiety, presumably because of the paramagnetic ion effect.

ESI-MS analysis of **2** showed peaks at $m/z = 182.54$ and 514.03 which were assigned to $[Fe(TPA)(F)]^{2+}$ and $[Fe(TPA)(F)(OTf)]^{+}$ (Figure S18). Given the nature of the anions in solution, either F^- or $^-$OTf could be the counterions for these ions in **2**. An ESI-MS of **2** generated from $HClO_4$ displayed two major peaks at $m/z = 464.03$ and 543.98 corresponding to the ions $[Fe(TPA)(F)(OClO_3)]^{+}$ and $[Fe(TPA)(OClO_3)_2]^{+}$, respectively (Figures S19–S21). These results lead us to conclude that **2** contains an $[Fe(TPA)(F)(X)]^{+}$ core structure where X is either F or OTf. The X anions could be bound to the Fe or could act as non-coordinating anions. Finally, the ESI-MS of **2** generated from $Sc^{III}(OTf)_3$ showed a dicationic peak at $m/z = 438.05$ which can be assigned to a scandium adduct with the formulation $[Fe(TPA)(F)_2Sc(OTf)_3]^{2+}$ (Figures S18, S22). Rational formal metal oxidation states for this ion would be Fe^{IV}/Sc^{III} or Fe^{III}/Sc^{IV} which are not in agreement with our EPR analysis of **2**. We therefore assume this species is derived from $[Fe^{III}(TPA)(F)\cdots Sc^{III}(OTf)_3]^{2+}$ and is formed in the mass spectrometer. ESI-MS analysis indicates that the elemental formulation of **2** is best defined as $[Fe(TPA)(F)(X)]^{+}$.

A comparison of the FT-IR of **1**, **2**, and $Sc^{III}(Otf)_3$ revealed a prominent peak at $\tilde{\nu} = 655\ cm^{-1}$ (putative asymmetric $\nu_{Fe-F-Fe}$) for **1** was absent in **2** (Figures S23, S24). This indicates the cleavage of a μ-Fe–F–Fe moiety leading to a mononuclear species. Additionally, the putative terminal ν_{Fe-F} peak at $\tilde{\nu} = 410\ cm^{-1}$ for **1** was shifted to $\tilde{\nu} = 417\ cm^{-1}$ for **2**. This may be associated with a Sc^{III} interaction with the F-atom in the newly formed terminal Fe–F bonds in **2** or simply a break-up of the dimer causing a modest shift in Fe–F stretch. We conclude that $Sc^{III}(Otf)_3$ cleaved the dimeric structure of **1**, yielding **2** with the formula $[Fe^{III}(TPA)(F)(X)]^{+}$; X = F/Otf, this structure is supported by EPR, NMR, FT-IR, and ESI-MS analyses.

*Hydrogen atom transfer reactivity by **2***: In comparison to **1**, **2** reacted readily with CHD. We explored the reactivity of **2** generated from $Sc^{III}(Otf)_3$ because when **2** was generated with $HclO_4$ it displayed short lifetimes making reactivity/kinetic studies unreliable (Figure S25). Upon addition of CHD (10 equiv.), the chromophore at $\lambda = 375$ nm converted to a broader absorption feature with $\lambda = 380$, 400 nm (Figure 4).

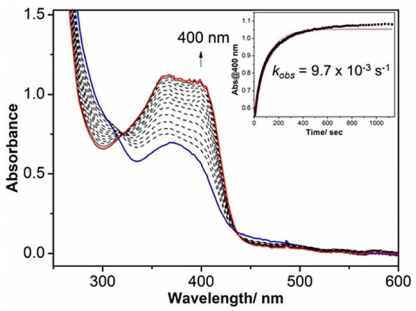

Figure 4. Electronic absorption spectra changes upon addition of CHD (350 equiv.) to **2** (0.1 mM, CH_3CN, at 0 °C). The inset shows the time profile of the feature at $\lambda = 400$ nm.

The species that formed was postulated to be the precursor complex $[Fe^{II}(NCCH_3)_2(TPA)]^{2+}$ by a comparison of their absorption spectra ($\lambda = 380$, 400 nm; Figure S11). This would indicate reduction of the Fe^{III} in **2** and loss of fluoride ligand, presumably as H–F. Pseudo-first order rate fitting for the decay of **2** was applied, by monitoring the changes at $\lambda =$ 400 nm over time, to obtain the rate of the reaction ($k_{obs} = 9.7 \times 10^{-3}\ s^{-1}$). A linear dependence of the k_{obs} with respect to [CHD] was observed yielding a plot with a slope = $0.15\ M^{-1}s^{-1}$ (Figure S26). This value corresponds to the reaction second-order rate constant k_2. The product of CHD oxidation was determined by ^1H NMR to be benzene (42 % yield; Figure S27). Yields of products were calculated based on one electron oxidation per iron atom (two iron atoms are consumed per molecule of benzene formation). The observed product is typical of PCET-mediated oxidation of CHD, where the removal of two formal hydrogen atoms yields benzene. **2** was thus a capable PCET oxidant of hydrocarbons.

We expanded the substrate scope by reacting **2** with xanthene, 9,10-dihydroanthracene (DHA), triphenylmethane, and cyclohexene. The formation of $[Fe^{II}(NCCH_3)_2(TPA)]^{2+}$ was observed in all cases according to UV/Vis (Figures S28–S31). For all substrates we measured k_{obs} and k_2 values (Figures S22–S31). Product analyses for each substrate were performed using gas chromatography (GC), NMR, or ESI-MS (see Supporting Information for details; Figures S32–S35). In no case did we observe fluorinated products, indicating that while **2** is a capable PCET oxidant, fluoride rebound did not occur. Product analysis indicated initial PCET oxidation of all substrates prior to conversion to other products.

A kinetic isotope effect (KIE) value of 2.1 was measured for **2** using DHA and DHA-D_4, ($k_2 = 1.45$ and $0.71\ M^{-1}s^{-1}$, respectively, Figure S36). This is within the classical range (2–7) and indicates that either a hydrogen atom or a proton was involved in the rate-limiting step.[5a,28] This further supports the mechanism that the rate-determining step is a PCET process. Similarly low KIE values were recently observed for high-valent metal oxidants, when there is no terminal oxo ligand.[5a,28]

We obtained the activation parameters ($\Delta H^{\ddagger} = 14 \pm 1$ kcal mol^{-1} $\Delta S^{\ddagger} = -17 \pm 4$ cal mol^{-1} K^{-1}) for C–H activation by **2** by performing an Arrhenius plot (−10 to 10 °C) for the reaction between **2** and CHD (Figure S37). These values are within the range for high-valent oxidants that perform PCET oxidation, in particular other high-valent metal–halides.[5b] Such large and negative $\Delta S^{\ddagger}$ values indicate that the HAT entity is the Fe–F complex rather than an F• radical. Mayer and co-workers have demonstrated that HAT reactions involving transition metal complexes typically display large reorganizational energy resulting in significant entropic ($\Delta S^{\ddagger} \gg 0$) contributions.[29] In contrast, HAT reactivity by simple radicals (X•) involves minimum reorganisation energy and hence $\Delta S^{\ddagger}$ would be close to zero.[30]

Having established that **2** was a capable PCET oxidant, we attempted to understand the mechanism of PCET oxidation by **2**. A plot of the free energy of activation ($\Delta G^{\ddagger}$), calculated from the respective k_2 values using the Eyring equation, against the substrate BDE_{C-H} can provide mechanistic insight (Figure 5). A slope of 0.27 was obtained which points towards a HAT or concerted proton and electron transfer (CPET) mechanism as per Marcus theory.[31] For an ideal HAT or CPET, a slope of 0.5 would be expected and for a non-concerted PCET mechanism a slope close to one is expected.[31b,32] Although the measured slope here is slightly less than the expected 0.5, there have been several reports of similar deviations for a HAT mechanism, and the value is comparable for those obtained for other high-valent metal–halides.[5a,c,11,31b,33]

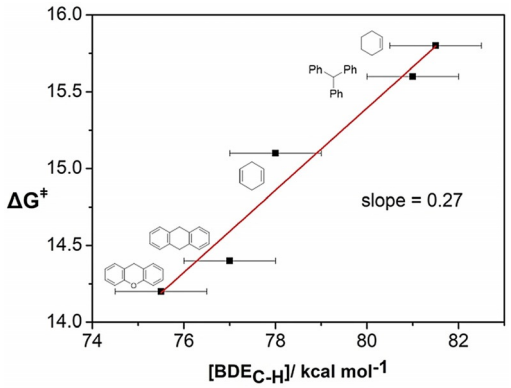

Figure 5. Plot of $\Delta G^{\ddagger}$ vs. BDE_{C-H}. $\Delta G^{\ddagger}$ was calculated using the Eyring equation from the corresponding k_2 values. We have plotted the BDE_{C-H} instead of bond dissociation free energy ($BDFE_{C-H}$) as the latter values for all the substrates in CH_3CN are not available.

2 is thus a mononuclear Fe^{III}–F oxidant that readily breaks C–H bonds through a HAT mechanism. $[Fe^{II}(NCCH_3)_2(TPA)]^{2+}$ was identified as the metal-based product of these reactions, leading us to conclude that H–F was the other product. We postulate that the strength of the H–F bond provides the driving force for oxidative C–H activation. As stated above, Fe^{III} oxidants that perform oxidative activation of C–H bonds are rare. **2** is a remarkably efficient oxidant when compared to well-established Fe^{III}–OR (R = H, alkyl) and Fe^{IV}=O oxidants (Table 1). In the oxidation of DHA, **2** displayed enhanced or comparable reactivity with the most reactive Fe^{III} oxidants reported to date, and compares well with both $S = 1$ and $S = 2$ Fe^{IV}=O oxidants. To the best of our knowledge, **2** represents the first Fe–F complex capable of

Table 1: Comparison of rate constants for the oxidation of DHA by Fe oxidants.

Complexes[a]	k_2 [$M^{-1}s^{-1}$]	T [°C]	Ref.
2	1.45	0	This work
$[Fe^{III}(OCH_3)(PY_5)]^{2+}$	1.2×10^{-4}	25	[11]
$[Fe^{III}(OH)(PY_5)]^{2+}$	4.3×10^{-4}	25	[13a]
$[Fe^{III}(OCH_3)(Hctb)]^{3+}$	9.8×10^{-4}	50	[13b]
$[Fe^{III}(OH)(OH_2)(PyPz)]^{4+}$	73	20	[13c]
$[Fe^{IV}(O)(N_4Py)]^{2+}$	18	25	[33a]
$[Fe^{IV}(O)(TMP)]$	2.7	−15	[34]
$[Fe^{IV}(O)(TMG_3tren)]^{2+}$	0.09	−30	[35]

[a] PY_5 = 2,6-bis(bis(2-pyridyl)methoxymethane)pyridine; Hctb = *N*,*N*,*N*′,*N*′-tetrakis(2-benzimidazolyl-methyl)orthodiamine-*trans*-cyclohexane; PyPz = tetramethyl-2,3-pyridino porphyrazine; N_4Py = *N*,*N*-bis(2-pyridyl)-*N*-bis(2-pyridyl)methylamine; TMP = tetramesitylporphinate; TMG_3tren = 1,1,1-tris{2-[*N*2-(1,1,3,3-tetramethylguanidino)]ethyl}-amine.

PCET oxidation. That it reacts at such high rates is an indicator that the strong H–F bond in the product is providing a high driving force for C–H activation.

Conclusion

We have presented the synthesis of an Fe^{III}(F)–F–Fe^{III}(F) complex (**1**) by reacting $[Fe^{II}(NCCH_3)_2(TPA)]^{2+}$ with difluoroiodobenzene. **1** presented sluggish reactivity in oxidative C–H activation. When Lewis or Brønsted acids were added to **1**, a mononuclear Fe^{III}–F complex was obtained (**2**). **2** was a remarkably reactive Fe^{III} reagent for oxidative C–H activation, demonstrating reaction rates for hydrocarbon oxidation comparable to the most reactive Fe^{III} and Fe^{IV} oxidants. A kinetic analysis suggested HAT was the mechanism of C–H activation. We postulate that the strength of the H–F bond in the product engenders the high reactivity observed in **2**. Further development of high-valent metal–fluorides is underway in our laboratory with the anticipation that the strong H–F bond could yield exceptionally reactive oxidants.

Acknowledgements

This publication has emanated from research supported by the European Research Council (ERC-2015-STG-678202). Research in the McDonald lab is supported in part by a research grant from Science Foundation Ireland (SFI/15/RS-URF/3307). We thank Prof. Robert Barklie for training on and use of an EPR spectrometer, Dr. John O'Brien and Dr. Manuel Ruether for help with NMR, and Dr. Gary Hessman for help with ESI-MS. Open access funding provided by IReL.

Conflict of Interest

The authors declare no conflict of interest.

Keywords: biomimetic chemistry · fluoride oxidant · high-valent oxidants · nonheme iron · proton-coupled electron transfer

[1] a) R. H. Crabtree, *Chem. Rev.* **2010**, *110*, 575; b) K. I. Goldberg, A. S. Goldman, *Acc. Chem. Res.* **2017**, *50*, 620–626; c) *Alkane Functionalization* (Eds.: A. J. L. Pombeiro, M. Fátima, C. G. da Silva), Wiley, Hoboken, **2019**.
[2] a) J. A. Labinger, J. E. Bercaw, *Nature* **2002**, *417*, 507–514; b) R. G. Bergman, *Nature* **2007**, *446*, 391–393.
[3] a) M. Costas, M. P. Mehn, M. P. Jensen, L. Que, *Chem. Rev.* **2004**, *104*, 939–986; b) J. T. Groves, *J. Inorg. Biochem.* **2006**, *100*, 434–447; c) W. Nam, *Acc. Chem. Res.* **2007**, *40*, 465; d) A. R. McDonald, L. Que, *Coord. Chem. Rev.* **2013**, *257*, 414–428; e) A. J. Jasniewski, L. Que, *Chem. Rev.* **2018**, *118*, 2554–2592.
[4] a) D. Dhar, W. B. Tolman, *J. Am. Chem. Soc.* **2015**, *137*, 1322–1329; b) M. K. Goetz, J. S. Anderson, *J. Am. Chem. Soc.* **2019**, *141*, 4051–4062.
[5] a) P. Mondal, P. Pirovano, A. Das, E. R. Farquhar, A. R. McDonald, *J. Am. Chem. Soc.* **2018**, *140*, 1834–1841; b) P. Mondal, M. Lovisari, B. Twamley, A. R. McDonald, *Angew. Chem. Int. Ed.* **2020**, *59*, 13044–13050; *Angew. Chem.* **2020**, *132*, 13144–13150; c) R. Gericke, L. M. Doyle, E. R. Farquhar, A. R. McDonald, *Inorg. Chem.* **2020**, *59*, 13952–13961.
[6] J. Berkowitz, G. B. Ellison, D. Gutman, *J. Phys. Chem.* **1994**, *98*, 2744–2765.
[7] a) B. J. Shields, A. G. Doyle, *J. Am. Chem. Soc.* **2016**, *138*, 12719–12722; b) S. K. Kariofillis, A. G. Doyle, *Acc. Chem. Res.* **2021**, *54*, 988–1000.
[8] D. Gygi, M. I. Gonzalez, S. J. Hwang, K. T. Xia, Y. Qin, E. J. Johnson, F. Gygi, Y.-S. Chen, D. G. Nocera, *J. Am. Chem. Soc.* **2021**, *143*, 6060–6064.
[9] a) L. Que, W. B. Tolman, *Nature* **2008**, *455*, 333–340; b) A. S. Borovik, *Chem. Soc. Rev.* **2011**, *40*, 1870–1874.
[10] a) F. H. Vaillancourt, E. Yeh, D. A. Vosburg, S. Garneau-Tsodikova, C. T. Walsh, *Chem. Rev.* **2006**, *106*, 3364–3378; b) W. Liu, J. T. Groves, *Acc. Chem. Res.* **2015**, *48*, 1727–1735; c) J. P. Biswas, S. Guin, D. Maiti, *Coord. Chem. Rev.* **2020**, *408*, 213174.
[11] C. R. Goldsmith, R. T. Jonas, T. D. P. Stack, *J. Am. Chem. Soc.* **2002**, *124*, 83–96.
[12] a) C. E. MacBeth, A. P. Golombek, V. G. Young, C. Yang, K. Kuczera, M. P. Hendrich, A. S. Borovik, *Science* **2000**, *289*, 938–941; b) E. M. Matson, Y. J. Park, A. R. Fout, *J. Am. Chem. Soc.* **2014**, *136*, 17398–17401; c) Z. Gordon, T. J. Miller, C. A. Leahy, E. M. Matson, M. Burgess, M. J. Drummond, C. V. Popescu, C. M. Smith, R. L. Lord, J. Rodríguez-López, A. R. Fout, *Inorg. Chem.* **2019**, *58*, 15801–15811.
[13] a) C. R. Goldsmith, T. D. P. Stack, *Inorg. Chem.* **2006**, *45*, 6048–6055; b) F. Mei, C. Ou, G. Wu, L. Cao, F. Han, X. Meng, J. Li, D. Li, Z. Liao, *Dalton Trans.* **2010**, *39*, 4267–4269; c) H. Gao, J. T. Groves, *J. Am. Chem. Soc.* **2017**, *139*, 3938–3941; d) P. Pirovano, A. R. McDonald, *Eur. J. Inorg. Chem.* **2018**, 547–560.
[14] E. Andris, R. Navrátil, J. Jašík, M. Puri, M. Costas, L. Que, J. Roithová, *J. Am. Chem. Soc.* **2018**, *140*, 14391–14400.
[15] Deposition number 2085806 (for **1**) contains the supplementary crystallographic data for this paper. These data are provided free of charge by the joint Cambridge Crystallographic Data Centre and Fachinformationszentrum Karlsruhe Access Structures service.
[16] K. Anzai, K. Hatano, Y. J. Lee, W. R. Scheidt, *Inorg. Chem.* **1981**, *20*, 2337–2339.
[17] a) S. C. Lee, R. H. Holm, *Inorg. Chem.* **1993**, *32*, 4745–4753; b) J. Vela, J. M. Smith, Y. Yu, N. A. Ketterer, C. J. Flaschenriem, R. J. Lachicotte, P. L. Holland, *J. Am. Chem. Soc.* **2005**, *127*,

7857 – 7870; c) D. Sil, A. Kumar, S. P. Rath, *Chem. Eur. J.* **2016**, *22*, 11214 – 11223.
[18] Y. Dong, H. Fujii, M. P. Hendrich, R. A. Leising, G. Pan, C. R. Randall, E. C. Wilkinson, Y. Zang, L. Que, *J. Am. Chem. Soc.* **1995**, *117*, 2778 – 2792.
[19] A. Ghosh, F. Tiago de Oliveira, T. Yano, T. Nishioka, E. S. Beach, I. Kinoshita, E. Münck, A. D. Ryabov, C. P. Horwitz, T. J. Collins, *J. Am. Chem. Soc.* **2005**, *127*, 2505 – 2513.
[20] S. B. Cherif, *Doctoral Thesis*, Universities of SFAX (Tunisia) and Oviedo (Spain), **2018**.
[21] a) D. L. Reger, A. E. Pascui, M. D. Smith, J. Jezierska, A. Ozarowski, *Inorg. Chem.* **2012**, *51*, 11820 – 11836; b) S. Dammers, T. P. Zimmermann, S. Walleck, A. Stammler, H. Bögge, E. Bill, T. Glaser, *Inorg. Chem.* **2017**, *56*, 1779 – 1782.
[22] a) S. Fukuzumi, Y. Morimoto, H. Kotani, P. Naumov, Y.-M. Lee, W. Nam, *Nat. Chem.* **2010**, *2*, 756 – 759; b) Y. Morimoto, H. Kotani, J. Park, Y.-M. Lee, W. Nam, S. Fukuzumi, *J. Am. Chem. Soc.* **2011**, *133*, 403 – 405; c) H. Yoon, Y.-M. Lee, X. Wu, K.-B. Cho, R. Sarangi, W. Nam, S. Fukuzumi, *J. Am. Chem. Soc.* **2013**, *135*, 9186 – 9194; d) J. Chen, Y.-M. Lee, K. M. Davis, X. Wu, M. S. Seo, K.-B. Cho, H. Yoon, Y. J. Park, S. Fukuzumi, Y. N. Pushkar, W. Nam, *J. Am. Chem. Soc.* **2013**, *135*, 6388 – 6391; e) M. Swart, *Chem. Commun.* **2013**, *49*, 6650 – 6652; f) S. Bang, Y.-M. Lee, S. Hong, K.-B. Cho, Y. Nishida, M. S. Seo, R. Sarangi, S. Fukuzumi, W. Nam, *Nat. Chem.* **2014**, *6*, 934 – 940; g) S. Hong, F. F. Pfaff, E. Kwon, Y. Wang, M.-S. Seo, E. Bill, K. Ray, W. Nam, *Angew. Chem. Int. Ed.* **2014**, *53*, 10403 – 10407; *Angew. Chem.* **2014**, *126*, 10571 – 10575; h) S. Fukuzumi, K. Ohkubo, Y.-M. Lee, W. Nam, *Chem. Eur. J.* **2015**, *21*, 17548 – 17559; i) J. Prakash, G. T. Rohde, K. K. Meier, A. J. Jasniewski, K. M. Van Heuvelen, E. Münck, L. Que, *J. Am. Chem. Soc.* **2015**, *137*, 3478 – 3481; j) S. H. Bae, Y.-M. Lee, S. Fukuzumi, W. Nam, *Angew. Chem. Int. Ed.* **2017**, *56*, 801 – 805; *Angew. Chem.* **2017**, *129*, 819 – 823; k) S. Kal, A. Draksharapu, L. Que, *J. Am. Chem. Soc.* **2018**, *140*, 5798 – 5804; l) Y. Liu, T.-C. Lau, *J. Am. Chem. Soc.* **2019**, *141*, 3755 – 3766.
[23] a) Z. Chen, L. Yang, C. Choe, Z. Lv, G. Yin, *Chem. Commun.* **2015**, *51*, 1874 – 1877; b) C. Choe, L. Yang, Z. Lv, W. Mo, Z. Chen, G. Li, G. Yin, *Dalton Trans.* **2015**, *44*, 9182 – 9192.
[24] a) W. E. Blumberg, J. Peisach, in *Bioinorganic Chemistry*, *Vol. 100*, American Chemical Society, Washington, **1971**, pp. 271 – 291; b) C. P. S. Taylor, *Biochim. Biophys. Acta. Protein Structure* **1977**, *491*, 137 – 148.
[25] a) K. Yamaguchi, Y. Watanabe, I. Morishima, *J. Am. Chem. Soc.* **1993**, *115*, 4058 – 4065; b) C. Kim, K. Chen, J. Kim, L. Que, *J. Am. Chem. Soc.* **1997**, *119*, 5964 – 5965; c) Y. Zang, J. Kim, Y. Dong, E. C. Wilkinson, E. H. Appelman, L. Que, *J. Am. Chem. Soc.* **1997**, *119*, 4197 – 4205; d) L. Duelund, R. Hazell, C. J. McKenzie, L. Preuss Nielsen, H. Toftlund, *J. Chem. Soc. Dalton Trans.* **2001**, 152 – 156; e) A. Mairata i Payeras, R. Y. N. Ho, M. Fujita, J. Que, *Chem. Eur. J.* **2004**, *10*, 4944 – 4953; f) E. A. Duban, K. P. Bryliakov, E. P. Talsi, *Mendeleev Commun.* **2005**, *15*, 12 – 14; g) W. N. Oloo, K. K. Meier, Y. Wang, S. Shaik, E. Münck, L. Que, *Nat. Commun.* **2014**, *5*, 3046.
[26] a) G. Roelfes, M. Lubben, K. Chen, R. Y. N. Ho, A. Meetsma, S. Genseberger, R. M. Hermant, R. Hage, S. K. Mandal, V. G. Young, Y. Zang, H. Kooijman, A. L. Spek, L. Que, B. L. Feringa, *Inorg. Chem.* **1999**, *38*, 1929 – 1936; b) O. Y. Lyakin, K. P. Bryliakov, E. P. Talsi, *Inorg. Chem.* **2011**, *50*, 5526 – 5538.
[27] S. Kobayashi, K. Manabe, *Acc. Chem. Res.* **2002**, *35*, 209 – 217.
[28] a) F. H. Westheimer, *Chem. Rev.* **1961**, *61*, 265 – 273; b) P. Pirovano, E. R. Farquhar, M. Swart, A. J. Fitzpatrick, G. G. Morgan, A. R. McDonald, *Chem. Eur. J.* **2015**, *21*, 3785 – 3790; c) P. Pirovano, E. R. Farquhar, M. Swart, A. R. McDonald, *J. Am. Chem. Soc.* **2016**, *138*, 14362 – 14370; d) T. Corona, A. Company, *Chem. Eur. J.* **2016**, *22*, 13422 – 13429; e) T. Corona, A. Draksharapu, S. K. Padamati, I. Gamba, V. Martin-Diaconescu, F. Acuña-Parés, W. R. Browne, A. Company, *J. Am. Chem. Soc.* **2016**, *138*, 12987 – 12996; f) G. Spedalotto, R. Gericke, M. Lovisari, E. R. Farquhar, B. Twamley, A. R. McDonald, *Chem. Eur. J.* **2019**, *25*, 11983 – 11990; g) C. McManus, P. Mondal, M. Lovisari, B. Twamley, A. R. McDonald, *Inorg. Chem.* **2019**, *58*, 4515 – 4523.
[29] a) E. A. Mader, E. R. Davidson, J. M. Mayer, *J. Am. Chem. Soc.* **2007**, *129*, 5153 – 5166; b) E. A. Mader, V. W. Manner, T. F. Markle, A. Wu, J. A. Franz, J. M. Mayer, *J. Am. Chem. Soc.* **2009**, *131*, 4335 – 4345.
[30] a) S. Rohe, A. O. Morris, T. McCallum, L. Barriault, *Angew. Chem. Int. Ed.* **2018**, *57*, 15664 – 15669; *Angew. Chem.* **2018**, *130*, 15890 – 15895; b) R. K. Neff, Y.-L. Su, S. Liu, M. Rosado, X. Zhang, M. P. Doyle, *J. Am. Chem. Soc.* **2019**, *141*, 16643 – 16650.
[31] a) J. P. Roth, J. C. Yoder, T.-J. Won, J. M. Mayer, *Science* **2001**, *294*, 2524 – 2526; b) J. M. Mayer, *Acc. Chem. Res.* **2011**, *44*, 36 – 46.
[32] J. J. Warren, T. A. Tronic, J. M. Mayer, *Chem. Rev.* **2010**, *110*, 6961 – 7001.
[33] a) D. Wang, M. Zhang, P. Bühlmann, L. Que, *J. Am. Chem. Soc.* **2010**, *132*, 7638 – 7644; b) D. Unjaroen, R. Gericke, M. Lovisari, D. Nelis, P. Mondal, P. Pirovano, B. Twamley, E. R. Farquhar, A. R. McDonald, *Inorg. Chem.* **2019**, *58*, 16838 – 16848.
[34] C. Fertinger, N. Hessenauer-Ilicheva, A. Franke, R. van Eldik, *Chem. Eur. J.* **2009**, *15*, 13435 – 13440.
[35] J. England, M. Martinho, E. R. Farquhar, J. R. Frisch, E. L. Bominaar, E. Münck, L. Que, Jr., *Angew. Chem. Int. Ed.* **2009**, *48*, 3622 – 3626; *Angew. Chem.* **2009**, *121*, 3676 – 3680.

Manuscript received: September 17, 2021
Accepted manuscript online: September 28, 2021
Version of record online: November 5, 2021

